Nanotechnology, Science and Applications

Dovepress

open access to scientific and medical research

Open Access Full Text Article

ORIGINAL RESEARCH

EGF Receptor-Targeting Cancer Therapy Using CD47-Engineered Cell-Derived Nanoplatforms

Moon Jung Choi[1], Kang Chan Choi[1], Do Hyun Lee[1], Hwa Yeon Jeong[1], Seong Jae Kang[1], Min Woo Kim[1], In Ho Jeong[1], Young Myoung You[1], Jin Suk Lee[2], Yeon Kyung Lee[1], Chan Su Im[1], Yong Serk Park[1]

[1]Department of Biomedical Laboratory Science, Yonsei University, Wonju, Republic of Korea; [2]Department of Anatomy, Yonsei University Wonju College of Medicine, Wonju, Republic of Korea

Correspondence: Chan Su Im; Yong Serk Park, Department of Biomedical Laboratory Science, Yonsei University, Wonju, Gangwon, 220-710, Republic of Korea, Email chanzzhu@nate.com; parkys@yonsei.ac.kr

Introduction: Avoiding phagocytic cells and reducing off-target toxicity are the primary hurdles in the clinical application of nanoparticles containing therapeutics. For overcoming these errors, in this study, nanoparticles expressing CD47 proteins inhibiting the phagocytic attack of immune cells were prepared and then evaluated as an anti-cancer drug delivery vehicle.

Methods: The CD47+ cell-derived nanoparticles (CDNs) were prepared from the plasma membranes of human embryonic kidney cells transfected with a plasmid encoding CD47. And the doxorubicin (DOX) was loaded into the CDNs, and anti-EGF receptor (EGFR) antibodies were conjugated to the surface of the CDNs to target tumors overexpressing EGFR.

Results: The CD47+iCDNs-DOX was successfully synthesized having a stable structure. The CD47+CDNs were taken up less by RAW264.7 macrophages compared to control CDNs. Anti-EGFR CD47+CDNs (iCDNs) selectively recognized EGFR-positive MDA-MB-231 cells in vitro and accumulated more effectively in the target tumor xenografts in mice. Moreover, iCDNs encapsulating doxorubicin (iCDNs-DOX) exhibited the highest suppression of tumor growth in mice, presumably due to the enhanced DOX delivery to tumor tissues, compared to non-targeting CDNs or CD47- iCDNs.

Discussion: These results suggest that the clinical application of biocompatible cell membrane-derived nanocarriers could be facilitated by functionalization with macrophage-avoiding CD47 and tumor-targeting antibodies.

Keywords: cell-derived nanoparticles, immune surveillance, CD47, doxorubicin, tumor targeting, cancer therapy

Introduction

Recently, a great deal of effort has been devoted to the development of precision medicine based on our understanding of disease genetics. An appropriate system for the delivery of effective therapeutics to target sites is a prerequisite for precision medicine. Many different types of delivery vehicles have been suggested and tested for precise and effective cancer treatments.[1] Among them, synthetic nanoparticles such as polymeric nanoparticles, liposomes, and metallic nanoparticles have been extensively investigated for clinical applications.[2–4] These nanoparticles could compensate for the disadvantages associated with free drug administration, inherent toxicity, poor therapeutic activity, and an absence of tumor specificity.[5] On the other hand, nanoparticles are easily recognized by the immune system in the body because of their xenobiotic characteristics, which results in rapid clearance in the blood circulation and a loss of pharmacokinetic properties.[6]

Recently, various nanoparticles originating from cell membranes have been studied.[7–9] Cell-derived nanoparticles (CDNs) can be biocompatible and invisible to the immune system depending on the constituents and conditions of preparation.[10] CDNs share the characteristics of original cell membranes because they possess the membrane proteins and lipid constituents of the original cells.[11] CDNs originating from erythrocyte plasma membranes have attracted research interest as they stay in the circulatory system for a long period of time.[12]

The long circulation of erythrocytes has been associated with CD47 expression in plasma membranes. CD47 is an integrin-associated protein (IAP) belonging to the immunoglobulin superfamily.[13] Also, it is known as a ligand of signal

Received: 29 December 2021
Accepted: 29 June 2022
Published: 5 July 2022

Graphical Abstract

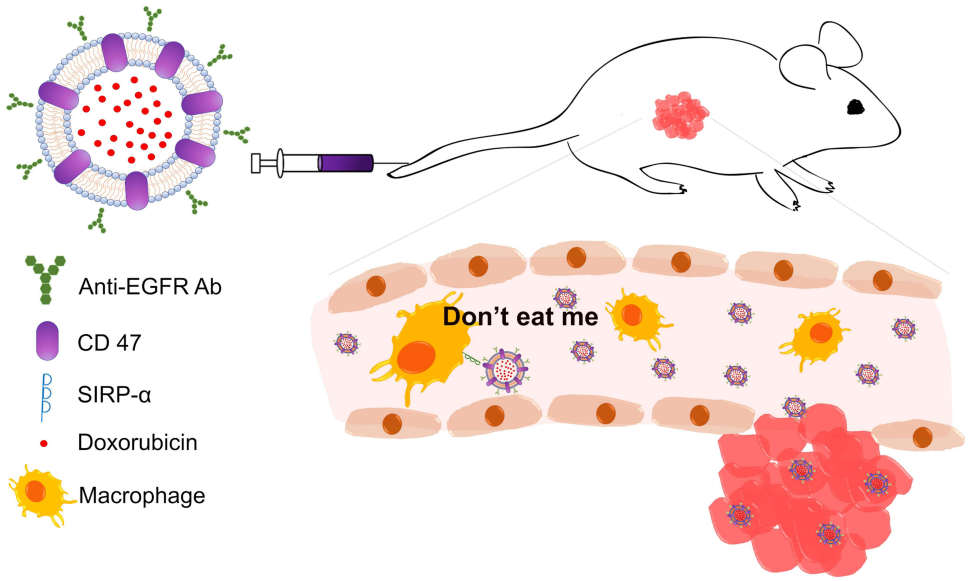

regulatory protein-alpha (SIRP-α) on macrophages, functioning as a "don't eat me" signal.[14] The interaction between CD47 and SIRP-α results in an escape from immune surveillance.[15] CD47 expressed on the tumor cell surface plays a key role in the establishment of tumor metastasis.[16] Recently, different types of nanoparticle functionalization by CD47 mimicry have been tested to avoid the immune surveillance system.[17]

For anticancer drugs and their delivery systems to be effective for cancer treatment, satisfying at least the following two conditions is necessary. First, after administration, the drug should reach the target tumor tissue, despite anatomical or immunological barriers, with minimal drug loss in the bloodstream. It is generally accepted that nanoparticle carriers selectively accumulate in tumor tissues through passive targeting, via the so-called enhanced permeability and retention (EPR) effect.[18] Second, the drug must selectively target tumor tissues and minimally affect normal tissues. Active targeting is an advanced strategy for cancer treatment to derive highly tumor-specific drug accumulation and low aberrant cytotoxicity.[19] Active tumor targeting has been performed by conjugating specific targeting ligands to the surface of nanoparticles.[20]

It has been well documented that the epidermal growth factor receptor (EGFR), the prototype of a class I family of receptor tyrosine kinases, is overexpressed or upregulated in various cancers, including colorectal, and brain, lung, and breast cancers.[19,21] Accordingly, anti-EGFR therapeutic antibodies have been developed to interfere with EGFR-induced signaling in cancer and are now being utilized in clinical settings.[22] In addition, antibodies against EGFR, such as cetuximab, have been extensively tested as cancer-targeting ligands for the active targeting of cancer cells overexpressing EGFR.[23–25]

In this study, novel CDNs were prepared from plasma membranes overexpressing CD47, which conferred the advantages of biocompatibility and long circulation in the blood. Furthermore, to provide active targeting capability, the anti-EGFR antibody cetuximab was coupled to the surface of the CDNs. Finally, doxorubicin (DOX) was loaded into the anti-EGFR immuno-CDNs which were then tested in vitro and in vivo to assess tumor targetability and therapeutic efficacy.

Results and Discussion

Preparation and Physicochemical Characterization of iCDNs

Recently, understanding the behavior and immunology of nanoparticles in vivo has provided a rationale for the development of biocompatible drug delivery systems,[26] such as CDNs made from red blood cells,[8] stem cells,[27] macrophages,[28] and cancer cells.[29] Based on this previous research, $CD47^+$ anti-EGFR immuno-CDNs encapsulating DOX ($CD47^+$ iCDNs-DOX) were conceptualized and prepared as illustrated in Figure 1A.

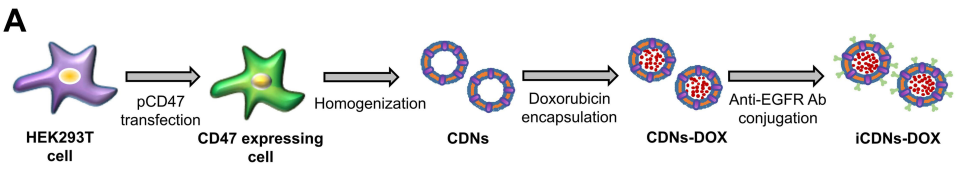

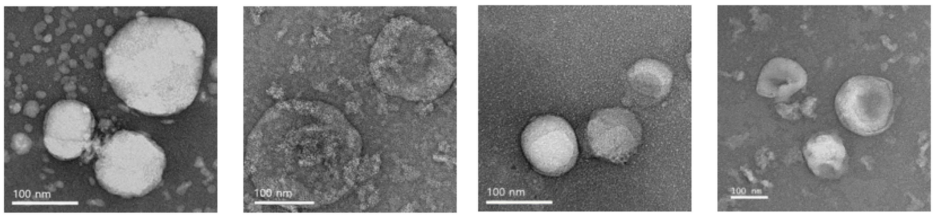

C

	Diameter (nm)	Zeta potential (mV)
CDNs	189.3 ± 6.6	-12.9 ± 1.2
iCDNs	207.2 ± 7.7	-12.5 ± 0.8
CDNs-DOX	228.6 ± 0.8	-14.5 ± 1.3
iCDNs-DOX	226.5 ± 15.3	-13.9 ± 0.7

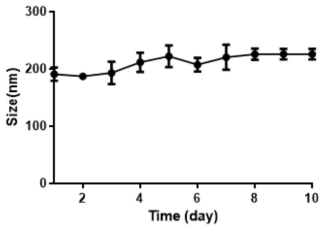

Figure 1 Preparation and characterization of CD47+ iCDNs-DOX. (**A**) The process of $CD47^+$ iCDNs-DOX preparation is illustrated. (**B**) The prepared $CD47^+$ CDNs, $CD47^+$ CDNs-DOX, $CD47^+$ iCDNs, and $CD47^+$ iCDNs-DOX (from left to right) were negatively stained with 2% uranyl acetate and then examined with a transmission electron microscope (×80 (K)). (**C**) The size and surface charge of the nanoparticles were analyzed three times with a ζ-sizer. Each diameter (nm) and zeta-potential represents the mean ± S.D. for three independent experiments. (**D**) The change of $CD47^+$ CDN size during storage at 4°C was monitored for 10 days. Each error bar represents the mean ± S.D. for three independent experiments.

First, HEK293T cells were transfected with the plasmid encoding CD47 (pCMV3-C-CD47GFPSpark, briefly pCD47GFP), and ample expression of CD47 on the transfected cells was verified by fluorescence microscopy (Figure S1). Nanoparticles were then formed by brief sonication of the harvested plasma membranes expressing CD47, followed by insertion of DSPE-PEG_{2000}-maleimide to provide coupling moieties for the antibody. Drug encapsulation into nanoparticles is a critical step in the development of nanocarriers for therapeutic drugs. In this study, DOX was efficiently encapsulated into the CDNs using a phosphate gradient created inside and outside the nanoparticles (Figure S2). The cumulative release of the loaded DOX was analyzed in PBS at 37°C. The $CD47^+$ CDN-DOX and $CD47^+$ iCDNs-DOX released DOX less than 30% of the total drug over 36 h (Figure S3). When the preformed CDNs and DOX were mixed at a 100:7 phospholipid: drug molar ratio, and then incubated for 48 h at room temperature, the structurally stable CDNs were able to encapsulate a large amount of DOX inside (19.6% loading efficiency). Finally, thiolated cetuximab antibodies were conjugated to the maleimide termini exposed on the surface of CDNs containing DOX to form $CD47^+$ iCDNs-DOX (Figure S4). According to TEM imaging (Figure 1B), all the prepared CDNs, DNS, CDNs-DOX, and iCDNs-DOX showed a stable vesicular nanostructure. The CDNs prepared by brief sonication in this study were smaller than 200 nm in diameter with narrow size distribution and were slightly negatively charged (−12.5 to −14.5 mV) (Figure 1C). DOX encapsulation and antibody conjugation hardly affected the integrity of the vesicular structure. The prepared $CD47^+$ iCDNs-DOX did not exhibit any serious size changes during their storage at 4°C for 10 days (Figure 1D). The size and negativity of CDNs may have some advantages concerning their sustained circulation in the blood and their passive targeting of tumors via the EPR effect.[30] The active targeting capability of nanoparticles is required for effective nano-bio interactions in the body. A variety of tumor-targeting ligands, such as antibodies, aptamers, peptides, and small molecules, have been conjugated to the surface of nanoparticles to facilitate a tumor-

recognizing capability.[31] A recent report demonstrated that cetuximab-conjugated nanodiamonds were capable of specifically targeting EGFR-overexpressing tumors.[19]

In vitro Macrophage Uptake of CDNs

HEK293T cells transfected with pCD47GFP efficiently expressed the fusion protein of CD47 and GFR on the plasma membranes, but not in the cytoplasm (Figure 2A). Western blot analysis also showed that the transfected cells, as well as the nanoparticles (CDNs) made of the plasma membranes of the transfected cells, contained a transiently expressed, ample amount of CD47 proteins (Figure 2B). To compare the $CD47^-$ CDNs and $CD47^+$ CDNs in terms of macrophage recognition, the nanoparticles were labeled with DiD hydrophobic fluorescence dye and then incubated with RAW 264.7 macrophage cells. Flow cytometric analysis showed that $CD47^-$ CDNs were more readily taken up by macrophages than $CD47^+$ CDNs (Figure 2C). Under the same experimental conditions, the macrophages incubated with the $CD47^+$ CDNs exhibited a smaller shift of fluorescence and lower mean fluorescence intensity compared to the cells incubated with the $CD47^-$ CDNs. Less interaction with macrophages became more obvious as time elapsed. The weak interaction of $CD47^+$ CDNs with macrophages may be due to the presence of the CD47 molecules. The CD47 exposed on the surface of nanoparticles could interact with SIRP-α on macrophages, resulting in an escape from the immune cells. The macrophage uptake of CDNs was also visualized by confocal microscopy (Figure 2D). Macrophages incubated with $CD47^-$ CDNs for 4 h showed more widespread and stronger fluorescence than those incubated with $CD47^+$ CDNs. This result also confirms the less binding of $CD47^+$ CDNs to macrophages, as observed in the previous cytometric analysis.

In vitro Tumor-Targeted Therapeutic Efficacy of iCDNs-DOX

For the preparation of tumor-targeting CDNs (anti-EGFR immuno-CDNs, referred to as iCDNs), the hydrated mixture of DSPE-PEG_{2000}-maleimide and DiD fluorescence dye was mixed with preformed $CD47^+$ CDNs by brief sonication. Thiolated cetuximab, an anti-EGFR antibody, was conjugated to the maleimide termini exposed on the surface of CDNs by direct coupling. Target tumor MDA-MB-231 cells expressing EGFR (Figure S5) were treated with $CD47^+$ iCDNs, and their specific interactions were verified using cytometric analysis (Figure 3A). CDNs deficient in targeting ligands were not able to effectively bind to target MDA-MB-231 or control MDA-MB-453 cells. However, the anti-EGFR iCDNs showed efficient binding to MDA-MB-231 cells, but not to MDA-MB-453 cells. This implies that the $CD47^+$ iCDNs can be specifically recognized by the target tumor cells, presumably via EGFR-mediated interactions. Previously, we reported that cetuximab is a useful tumor-targeting molecule for TNBC cells.[32]

To verify the tumor-targeted drug delivery of $CD47^+$ iCDNs, DOX was loaded into the prepared CDNs using the phosphate gradient method. Under the optimized conditions, incubation of DOX and CDNs (1 mM of lipid:40 μg of DOX) at 37°C for 48 h in the presence of 300 mM ammonium phosphate in the extravesicular medium was performed, and the highest amount of DOX (20%) was encapsulated into CDNs, and the structural integrity of CDNs was stably maintained thereafter. Thiolated cetuximab was then conjugated to the surface of the $CD47^+$ CDNs encapsulating DOX, as described above, referred to as $CD47^+$ iCDN-DOX. According to the confocal microscopic analysis (Figure 3B), MDA-MB-231 cells treated with $CD47^+$ iCDNs-DOX exhibited stronger DOX fluorescence than MDA-MB-453 cells under the same experimental conditions. This implies that $CD47^+$ iCDNs-DOX were able to deliver DOX more effectively to the cytoplasm of the target MDA-MB-231 cells than that of the non-target MDA-MB-453 cells. The enhanced delivery of DOX could be due to the specific recognition of $CD47^+$ iCDN-DOX via interactions between cetuximab and EGF receptors. Presumably, the specific recognition of $CD47^+$ iCDNs-DOX would be immediately followed by endocytosis of the nanoparticles because the EGF receptor is one of the most efficient endocytic receptors.[33] This phenomenon has also been demonstrated in several previous reports. For example, formulations of lipid nanoparticles conjugated with cetuximab antibodies were able to efficiently deliver quantum dots,[34] oligonucleotides,[35] or chemical drugs[36] to target cells.

Next, the cytotoxicity of $CD47^+$ iCDNs-DOX to MDA-MB-231 and MDA-MB-453 cells was compared with that of free DOX and non-targeting $CD47^+$ CDN-DOX. It is generally accepted that the encapsulation of therapeutics into membranous vesicles tends to reduce the in vitro cytotoxicity of free drugs.[37] According to the CCK-8 assay, encapsulation into iCDNs or CDNs significantly affected the cytotoxicity of DOX in the MDA-MB-453 cells

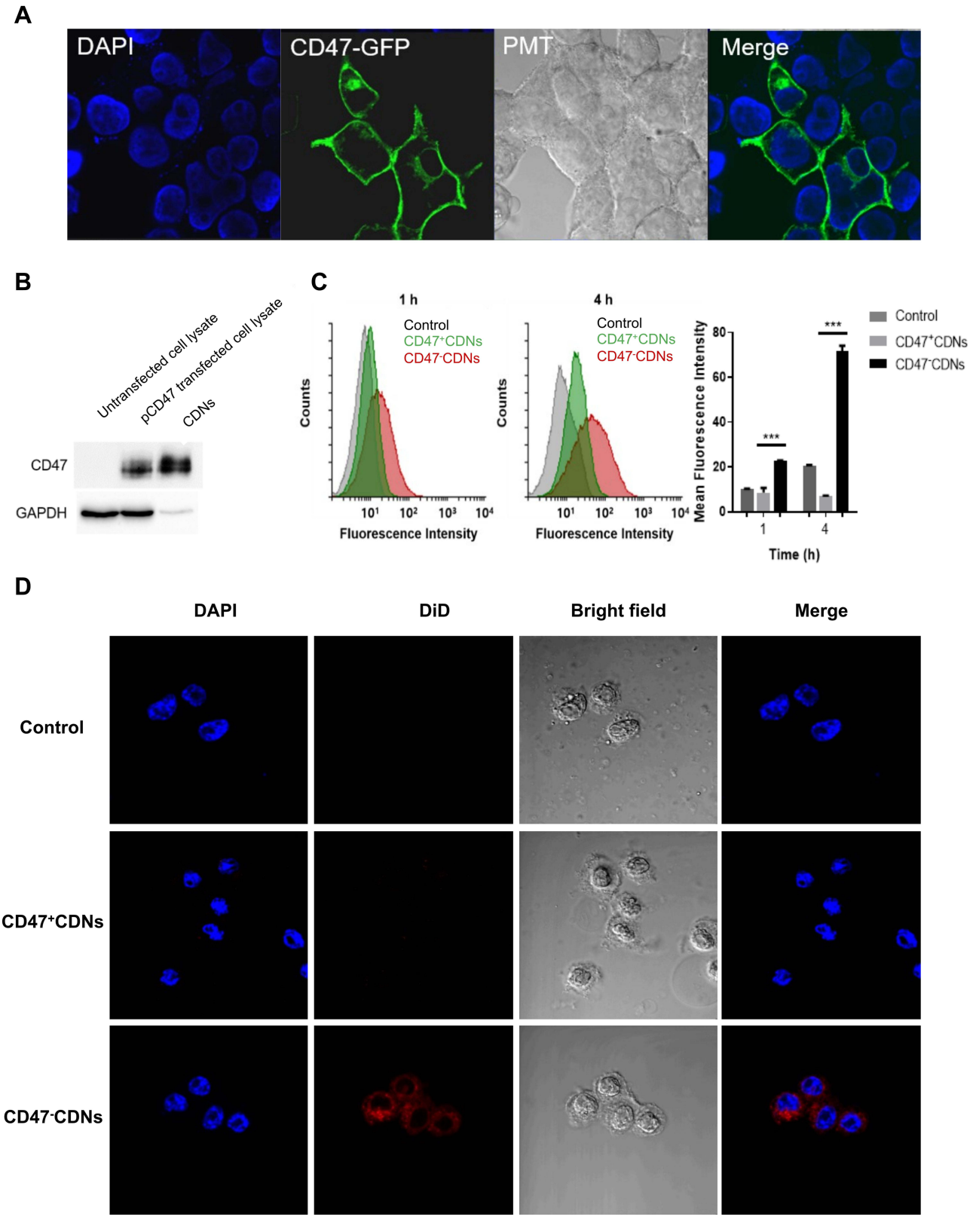

Figure 2 Interaction of CDNs with macrophages. (**A**) The expression of CD47-GFP fusion protein on the cell surface was identified using a confocal microscope (×800). (**B**) Western blotting of transfected cell lysates and CDNs verified the CD47 presence. (**C**) RAW264.7 cells were treated with DiD-labeled $CD47^{-}$ CDNs or $CD47^{+}$ CDNs for 1 or 4 h, and then subjected to flow cytometry. (**D**) The macrophages incubated with CDNs for 4 h were also examined with a confocal microscope (×800). ***, $p<0.001$ vs cells treated with CDNs. Each error bar represents the mean ± S.D. for three independent experiments.

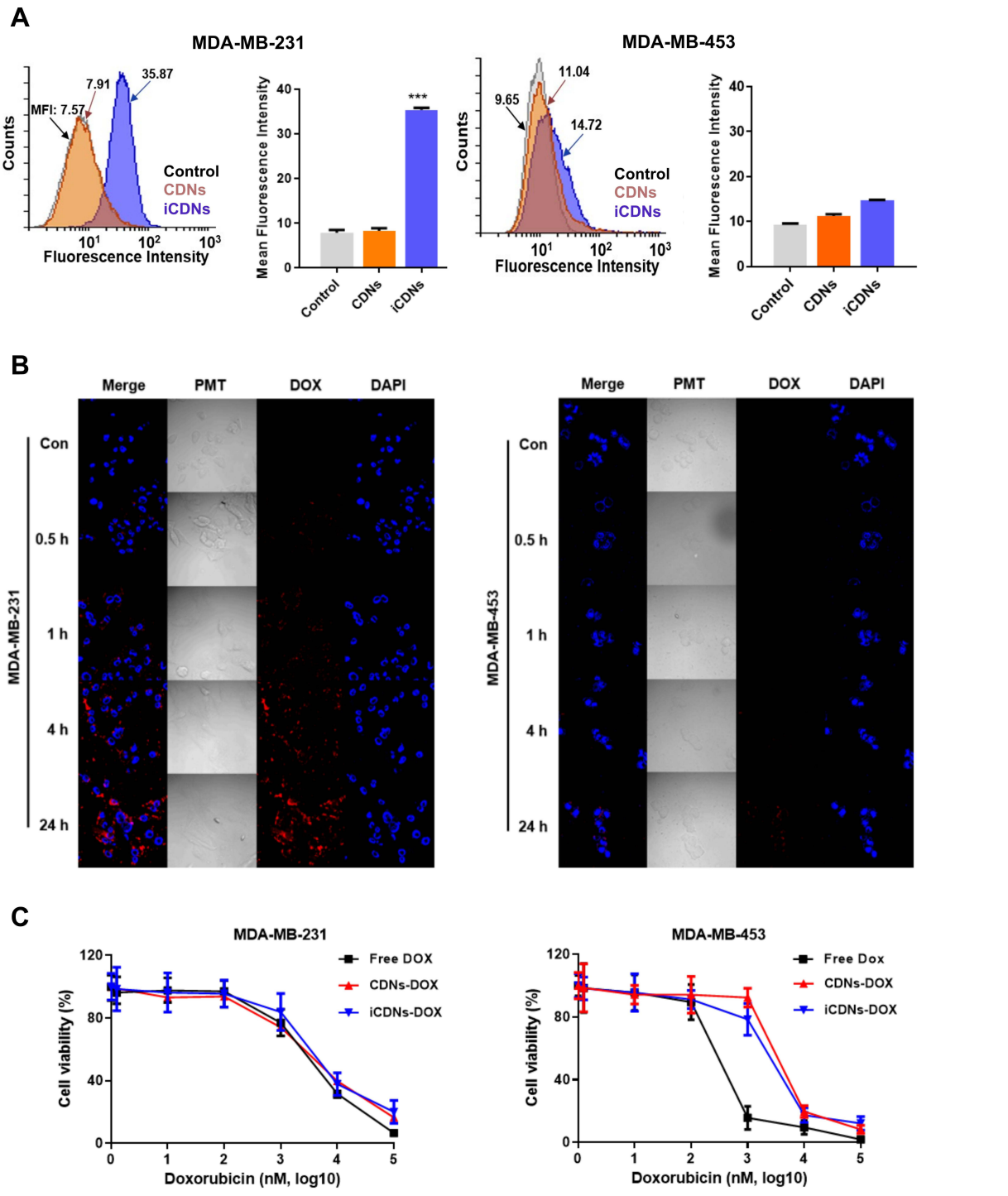

	Free DOX	CDNs-DOX	iCDNs-DOX
IC_{50} (μM)	4.05 ± 1.07	4.20 ± 0.95	3.77 ± 1.51

	Free DOX	CDNs-DOX	iCDNs-DOX
IC_{50} (μM)	0.32 ± 0.1	3.02 ± 1.46	2.11 ± 0.62

Figure 3 EGFR-specific cell biding of CD47+ iCDNs and tumor targeting and cytotoxicity of CD47+ iCDNs-DOX. (**A**) MDA-MB-231 and MDA-MB-453 cells were treated with Alexa fluor 488-labeled $CD47^+$ iCDNs and then subjected to FACS analysis (upper). (**B**) MDA-MB-231 and MDA-MB-453 cells were treated with $CD47^+$ iCDNs-DOX and stained with DAPI. The treated cells were examined with a confocal microscope at various time points. PMT, photomultiplier tube. (**C**) The tumor cells were also treated with various concentrations of DOX in a free form, $CD47^+$ CDNs, or $CD47^+$ iCDNs for 48 h, and the cell viability was quantified using the CCK-8 assay. The mean fluorescence of the treated cells was calculated (n=5) (bottom). ***, $p<0.001$ vs cells treated with CDNs. Each error bar represents the mean ± S.D. for three separate experiments.

(Figure 3C). The IC_{50} of free DOX in the MDA-MB-453 cells was 0.32 ± 0.10 μM while those of $CD47^+$ CDNs-DOX and $CD47^+$ iCDNs-DOX were 3.02 ± 1.46 μM and 2.11 ± 0.62 μM, respectively. Meanwhile, in MDA-MB-231 cells, the IC_{50} of free DOX (4.05 ± 1.07 μM) was insignificantly changed by encapsulation into $CD47^+$ CDNs (4.20 ± 0.95 μM) or $CD47^+$ iCDNs (3.77 ± 1.51 μM). CoThe couplingf tumor-targeting cetuximab to the surface of $CD47^+$ CDNs-DOX did not significantly enhance the in vitro cytotoxicity of the encapsulated drug. In confined wells for cell culture, free drugs may have advantages in terms of accessibility and penetration into the cell via various endocytic pathways such as pinocytosis, compared to vesicles encapsulating drugs.

In vivo Biodistribution of iCDNs in Tumor-Bearing Mice

To evaluate the biodistribution pattern of the $CD47^+$ iCDNs, mice were xenografted with MDA-MB-231 cells and then intravenously injected with DiO-labeled $CD47^+$ CDNs or $CD47^+$ iCDNs. Tumor tissues and major organs (eg, the liver, lung, heart, kidney, spleen, and blood) were collected and fluorescence images were taken with an imaging system at 10 min and 1, 4, 24, and 48 h post-injection (Figure 4). Mice treated with $CD47^+$ iCDNs showed relatively stronger fluorescence signals from tumor tissues at the right mammary fat pad, compared to those treated with $CD47^+$ CDNs (Figure 4A). Stronger fluorescence from tumor xenografts was consistent throughout all measurements. After in vivo imaging analysis, major organs (liver, lungs, kidneys, spleen, and tumor) were dissected from the mice and their ex vivo fluorescence images were taken as well (Figure 4B). At the same time point, the $CD47^+$ iCDN-treated group showed more intense fluorescence signals from the tumors than the $CD47^+$ CDN-treated group. Fluorescence from the liver was generally stronger in the CDN group. The tumor fluorescence signal in the $CD47^+$ CDN-treated group was low at 10 min post-injection and then became the highest 4 h later, followed by gradual dissipation of the signal. However, the tumor fluorescence signal in the $CD47^+$ iCDN group was strong even 10 min after injection and maintained a high level

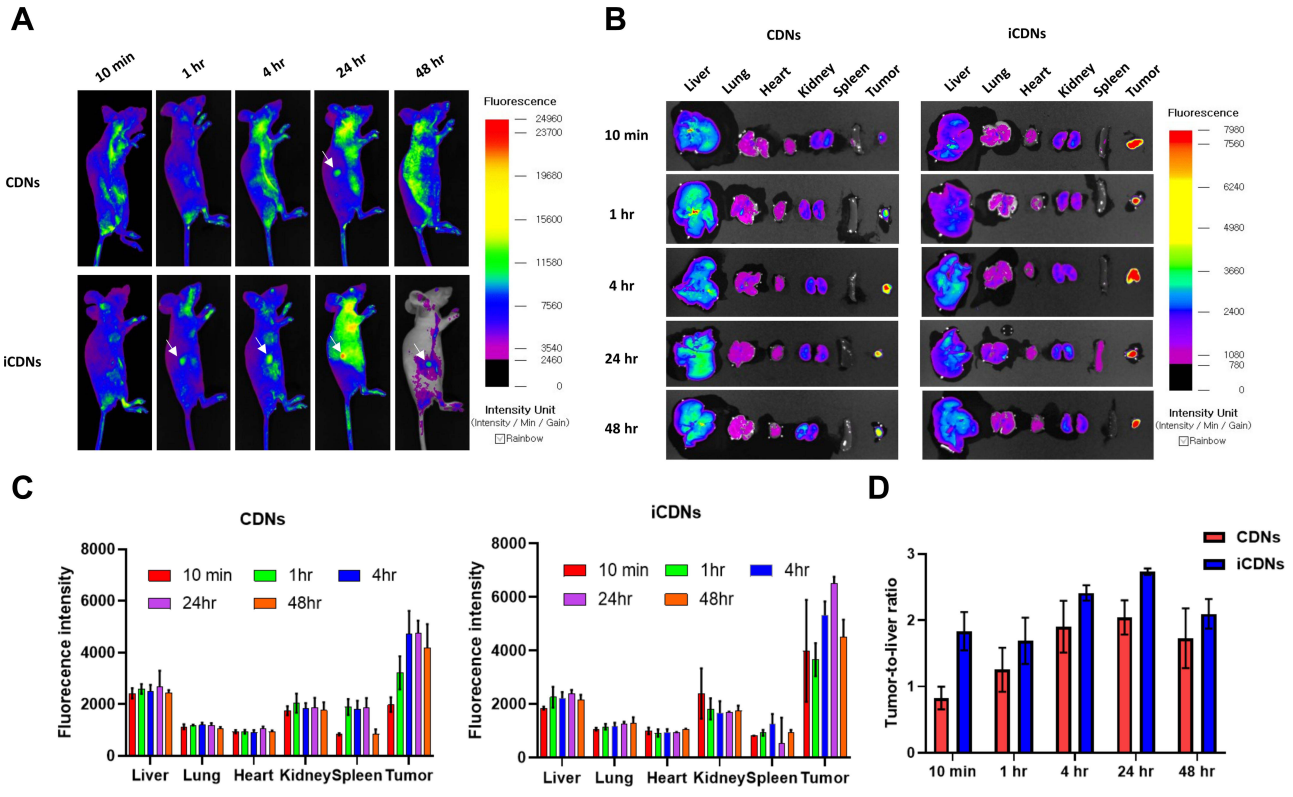

Figure 4 Biodistribution of CD47+ iCDNs in MDA-MB-231-xenografted mice. (**A**) The mice bearing MDA-MB-231 tumors were intravenously injected with DiO-labeled $CD47^+$ CDNs or $CD47^+$ iCDNs. (**B**) The whole-body fluorescence images were taken with an in vivo imaging system Then, major organs were removed, and the fluorescence images of the organs were also taken. (**C**) The relative fluorescence intensities of the organs at each time point were calculated by dividing the measured fluorescence intensity by area. (**D**) Tumor-to-liver ratios of $CD47^+$ CDNs and $CD47^+$ iCDNs were compared to each other at the same time point. Each error bar represents the mean ± S.D. of three measurements.

of fluorescence intensity for 48 h. The relative fluorescence intensity of the organs (Figure 4C), which was calculated by dividing the total fluorescence intensity by area, also showed the same tendency as that of the $CD47^+$ CDNs and $CD47^+$ iCDNs. Additionally, a relatively higher uptake by the spleen was observed in the CDN group. To compare the tumor targetability of the $CD47^+$ CDNs and $CD47^+$ iCDNs, a tumor-to-liver ratio (TLR) was calculated from each measurement (Figure 4D). According to the calculation, the TLRs in the $CD47^+$ iCDN group were generally higher than those in the CDN group. The improved TLRs of $CD47^+$ iCDNs could be presumably due to the efficient extravasation from the circulation and their active target cell recognition followed by efficient EGFR-mediated endocytosis of the particles.[38]

In vivo Tumor Growth Inhibition by $CD47^+$ iCDNs-DOX

To evaluate the anti-cancer therapeutic efficacy of $CD47^+$ iCDNs-DOX, mice carrying MDA-MB-231 tumors were intravenously injected with $CD47^+$ iCDNs-DOX thrice at three-day intervals (Figure 5A), and their tumor growth was

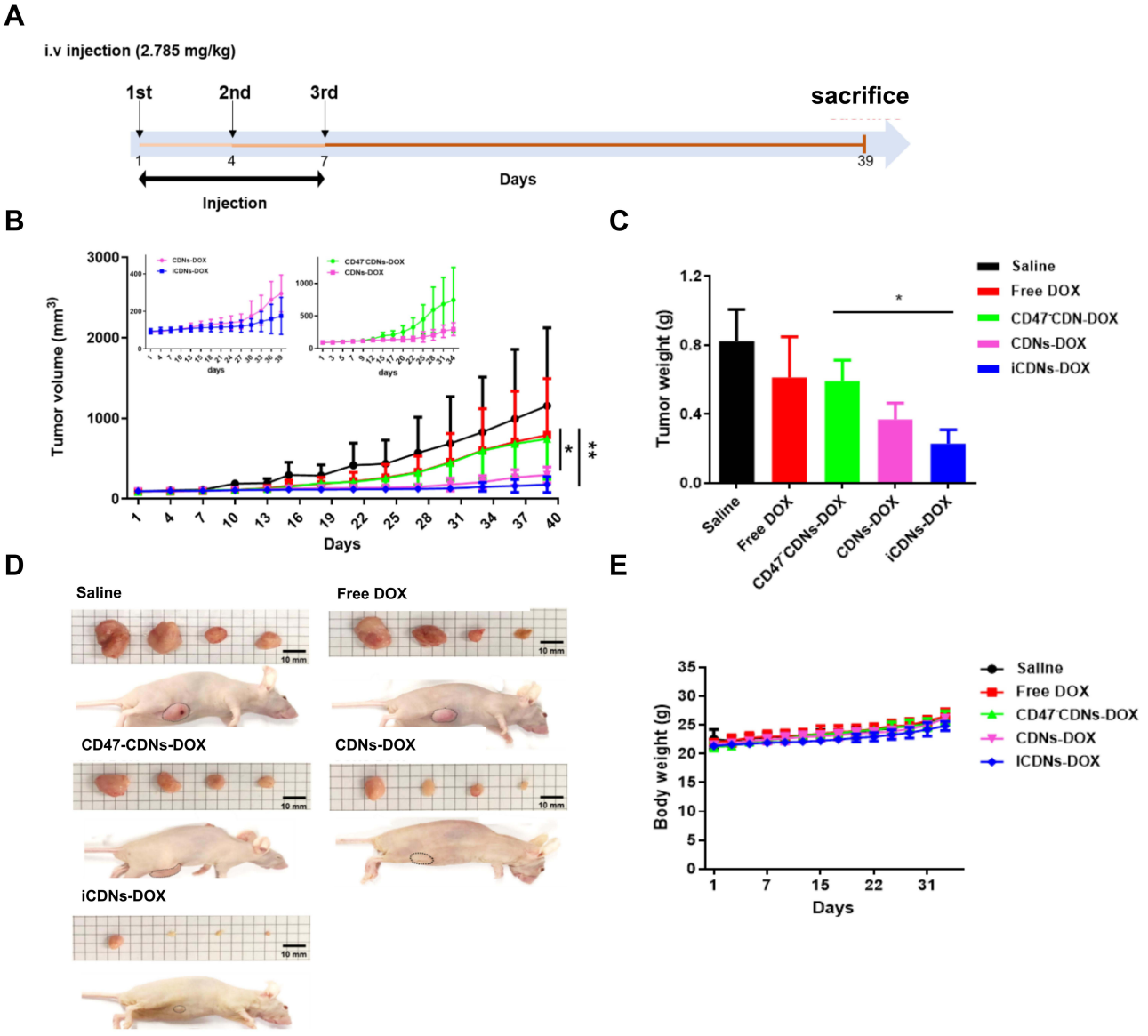

Figure 5 Suppression of in vivo tumor growth by a series of CDNs-DOX. (**A**) MDA-MB-231 cells were subcutaneously implanted into mice, which were then intravenously injected with saline, free DOX, $CD47^-$ CDNs-DOX, $CD47^+$ CDNs-DOX, or $CD47^+$ iCDNs-DOX at days 1, 4, and 7. (**B**) Tumor volumes were measured once every 3–4 days. (**C** and **D**) On day 39, the tumors were excised and weighed. (**E**) The body weights of the mice were also measured on the measurement days. Each error bar represents the mean ± S.D. (n=4). *, $p<0.05$ and **, $p<0.01$ vs $CD47^-$ CDNs-DOX-injected group.

compared with that of mice treated with control drugs such as free DOX, $CD47^-$ CDNs-DOX, and CD47+ CDNs-DOX for 39 days (Figure 5B). Overall, the anti-EGFR iCDNs-DOX exhibited the most effective inhibition of tumor growth among the treatment groups. Even though the untargeted $CD47^+$ CDNs-DOX showed stronger tumor growth inhibition than free DOX and $CD47^-$ CDNs-DOX, the tumor-targeted $CD47^+$ iCDNs-DOX showed the least tumor growth. However, the difference between the tumor-targeted and untargeted tumors was statistically insignificant during the treatment period. The weights of tumors excised at the last day also showed the best effectiveness of the $CD47^+$ iCDNs-DOX in the inhibition of tumor growth (Figure 5C and 5D).

Meanwhile, the free drug-treated or $CD47^-$ CDNs-DOX-treated mice showed similar tumor weights (0.613 ± 0.240 mg and 0.593 ± 0.240 mg, respectively). As stated above (Figure 5B), the tumor weights of $CD47^+$ iCDNs-DOX-treated mice were lower (0.228 ± 0.163 mg) than those of $CD47^+$ CDNs-DOX-treated mice (0.370 ± 0.189 mg). These results imply that the immune cell-avoiding CD47 proteins and tumor-targeting cetuximab molecules exposed on the surface of the CDNs may synergistically enhance the intracellular delivery of DOX into the cytoplasm of tumor cells, resulting in the elevation of the anticancer therapeutic efficacy of the nanocarrier system. Meanwhile, the membrane nanocarrier systems themselves did not show any serious in vivo toxicity during the treatment (Figure 5E). All the mice systemically treated with the membrane nanoparticles containing DOX or free DOX did not show any acute bodyweight loss, which could be caused by their inherent adverse toxicities. These data verify that this type of membrane nanoparticle system can be safely translated to the clinic if its merits as a drug delivery system are fully substantiated by further systematic preclinical tests.

Histology of Mice Treated with CD47+ iCDNs-DOX

At the endpoint of tumor growth measurement, major organs and tissues such as the heart, kidneys, liver, lungs, and tumor tissues were excised and subjected to histological analyses (Figure 6). It has been well-documented that free DOX

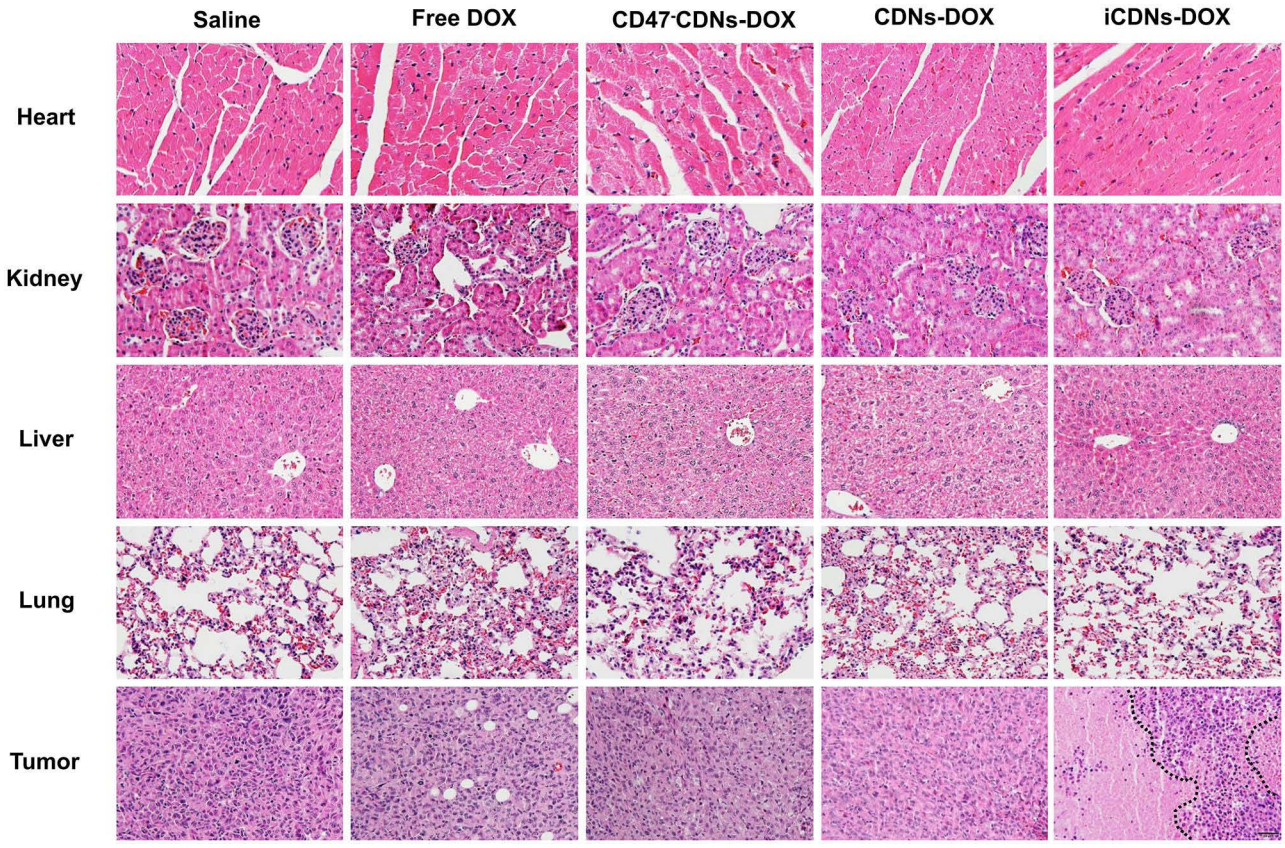

Figure 6 Histopathology of the major organs of mice treated with a series of CDNs-DOX. Tumors and major organs including the heart, kidneys, liver, and lungs were removed and dissected on day 39 post-injection of saline, free DOX, $CD47^-$ CDNs-DOX, $CD47^+$ CDNs-DOX, or $CD47^+$ iCDNs-DOX. The organs were embedded in paraffin, sliced, and then hematoxylin and eosin (H&E)-stained. The black dotted lines in the tumor pictures show the necrosis area (bright pink).

may induce a certain level of cardiac toxicity at a high dosage.36 However, compared with the saline-treated control mice, all the groups of treated mice showed no significant adverse morphological changes in the heart tissues at the test dose of DOX (2.8 mg/kg). In addition, no serious histological changes were detected in the sliced tissues of the liver, kidneys, and lungs.

Interestingly, broad necrotic areas were observed in the tumor tissues of the mice treated with $CD47^-$ CDNs-DOX, $CD47^+$ CDNs-DOX, or $CD47^+$ iCDNs-DOX. However, the saline- or free DOX-treated mice showed the typical histology of aggressively grown tumors, representing irregular nucleic positions and many blood vessels throughout the tissue. However, the tumor tissues treated with the series of CDNs-DOX exhibited a certain extent of tissue necrosis and infiltrated inflammatory cells. These results indicate that the cell membrane-derived nanoparticles may have stronger tumor tropism, facilitating a more efficient delivery of drugs compared to the delivery of the free drug to the target tumor site. In addition, the tumor-targeting cetuximab and CD47 molecules exposed on the surface of the nanoparticles may have a synergistic (or additive) positive impact on the inhibition of the growth of the target tumor tissue. These results also imply that cell-derived nanocarriers exposing CD47 and anticancer ligands could be accepted as a new drug delivery system for targeted cancer therapy.

Conclusion

In this study, a novel tumor-targeting nanocarrier system, namely the CD47-expressing anti-EGFR cell-derived nanoparticles ($CD47^+$ iCDNs), was successfully formulated by sequential preparation steps, which were as follows: i) CD47 transfection, ii) CDN preparation with CD47-expressing plasma membranes, iii) successful DOX encapsulation into the CDNs, and iv) conjugation of anti-EGFR antibodies on the CDN surface. The resulting $CD47^+$ iCDNs accumulated more efficiently in the target tumor tissues than the untargeted CDNs. In addition, $CD47^+$ iCDNs containing DOX exhibited the highest inhibitory effect on the growth of the target tumor tissue in vivo compared with the other formulations of CDNs. The enhanced targeting to tumors and the elevated tumor growth inhibition by the $CD47^+$ iCDNs was presumably due to the CD47-mediated immune cell avoidance, in addition to the EGFR-mediated active interactions with the target tumor cells. These results show that the $CD47^+$ iCDNs are stable, biocompatible, less immunogenic, and effective tumor-targeting vehicles for the tumor-targeted delivery of anticancer drugs in vivo. A further in depth systematic preclinical evaluation of $CD47^+$ iCDNs on a larger scale would verify the usefulness of the $CD47^+$ iCDN system as a potential drug carrier for targeted cancer therapy.

Experimental Section

Materials

1.2-Distearoyl-sn-glycero-3-phosphoethanolamine-N-maleimide (polyethylene glycol)-2000] ($DSPE\text{-}PEG_{2000}$-maleimide) and 1-palmitoyl-2-oleoyl-sn-glycero-3-phosphocholine (POPC) were purchased from Avanti Polar Lipid, Inc. (Alabaster, AL, USA). *O,O*-dimyristyl-N-lysyl glutamate (DMKE) cationic lipid was purchased from KOMA Biotech (Seoul, South Korea). The mouse CD47 ORF cDNA clone expression plasmid, C-GFPSpark tag (pCD47-GFP), was purchased from Sino Biological Inc. (Beijing, China). DOX was purchased from Sigma-Aldrich (St. Louis, MO, USA). Anti-EGFR antibodies (cetuximab, Erbitux®) were purchased from Merck KgaA (Darmstadt, Germany). Matrigel was purchased from Corning (New York, NY, USA).

Cell Lines and Culture

HEK293T (human embryonic kidney; CRL-3216™), MDA-MB-231 (human breast metastatic carcinoma, HTB-26™), MDA-MB-453 (human breast metastatic carcinoma, HTB-131™), and RAW264.7 (murine macrophage, TIB-71™) cell lines were purchased from the American Type Culture Collection (Manassas, VA, USA). HEK293T and RAW264.7 cells were maintained in Dulbecco's modified Eagle's medium (DMEM; Gibco, Carlsbad, CA, USA) supplemented with 10% fetal bovine serum (FBS, Gibco), 100 IU/mL penicillin (Gibco), and 100 μg/mL streptomycin (Gibco) in a humidified atmosphere of 95% air and 5% CO_2 at 37 °C. MDA-MB-231 and MDA-MB-453 cells were maintained in Leibovitz's

L-15 medium (Gibco) supplemented with 10% fetal bovine serum, 100 IU/mL penicillin, and 100 μg/mL streptomycin in a humidified, CO_2-free atmosphere at 37 °C.

Animals

All animal experiments were approved by the Institutional Animal Care and Use Committee (IACUC) of Yonsei University at Wonju (YWCI-201805-006-01) and performed under protocols in accordance with the school guidelines and regulations.

Preparation of $CD47^+$-CDNs

The plasmid encoding CD47 was transfected into human embryonic kidney (HEK293T) cells. Cells were cultured in a 60-mm cell culture dish to 70% confluence. pCD47-GFP and DMKE (1:3 weight ratio) were mixed in Opti-MEM for 30 min before transfection. The cells were treated with the mixed transfection solution and incubated for 48 h.

To extract plasma membranes, pCD47-transfected cells were detached with 5 mM EDTA-4Na in PBS (Sigma-Aldrich, St. Louis, MO, USA) by centrifugation at 200 ×g for 3 min, and the cells were washed with PBS. The cells were then suspended in a hypotonic solution buffer containing 20 mM Tris-HCl, 3 mM $MgCl_2$, and 10 mM NaCl at 4°C, followed by homogenization using a Dounce homogenizer. After centrifugation at 5000 ×g for 10 min at 4°C, the supernatant was collected and centrifuged again at 15,000 ×g for 30 min at 4°C. The supernatant was discarded, and the pellet was dispersed in PBS (pH 7.4). The suspended pellet was sonicated three times for 20s at 22% amplitude using a VibraCell VC50 (Sonics & Materials Inc., Danbury, CT, USA) on ice. The resulting cell-derived nanoparticles were stored at 4°C for further experiments. The amounts and concentrations of CDNs were expressed as the ones of phospholipids consisting in the prepared CDNs, quantified by the phosphate assay with a reference of POPC.[39]

For antibody conjugation, DSPE-PEG_{2000}-maleimide (1 mg, 0.34 μmole) was dried under N_2 gas and hydrated with 1 mL of buffer to prepare a micelle solution. The DSPE-PEG_{2000}-maleimide micelle solution (4 nmole) was added to the cell-derived nanoparticles (1 μmole of phospholipids) and then sonicated for 10s three times on the ice. The prepared DSPE-PEG_{2000}-maleimide-incorporated $CD47^+$-CDNs are referred to as Mal-$CD47^+$-CDNs.

DOX Encapsulation into CDNs

DOX was encapsulated into CDNs using the phosphate gradient method[40] with minor modifications. CDNs were prepared in ammonium phosphate buffer (300 mM, pH 7.4) and then passed through a PD-10 column (GE Healthcare, Chicago, IL, USA) for exchange with HEPES-EDTA buffer (25 mM, 140 mM NaCl, 2 mM EDTA, pH 7.4). The prepared $CD47^+$ CDNs (1 mL of 1 mM phospholipids) were incubated in the presence of 40 μg/mL of DOX for various periods at 37°C. After incubation, free DOX was removed from the $CD47^+$ CDNs containing DOX ($CD47^+$ CDNs-DOX) by passing through a PD-10 column. The loaded amounts of DOX were quantified by measuring the absorbance of DOX at 480 nm.

Cetuximab Conjugation to CDNs-DOX

To provide reactive thiol groups, 1 mg cetuximab was thiolated for 1 h at room temperature by reacting with 4.6 μL of 2 mg/mL of Traut's reagent (Thermo Scientific, Rockford, IL, USA). Unreacted Traut's reagents were removed using a PD-10 desalting column. The thiolated antibodies were added to the Mal-$CD47^+$-CDNs-DOX at a molar ratio of 0.2:1 (antibody: DSPE-PEG_{2000}-maleimide), and the mixture was incubated for 16 h at 4°C. Unconjugated antibodies were removed using sepharose CL-4B columns in HEPES-EDTA buffer (pH 7.4). The antibody conjugation to $CD47^+$ CDNs was confirmed by 10% PAGE.

Characterization of CDNs

The size and surface charge of the CDNs were measured using a dynamic light scattering zeta-sizer (Nano-ZS90, Malvern Instruments Ltd. Malvern, UK). These measurements were repeated three times.

The morphology of the CDNs was observed using transmission electron microscopy (TEM) (JEM-2100F, JEOL Ltd, Tokyo, Japan). CDNs and CDNs-DOX (1 nM) were loaded onto a carbonyl-coated 400-mesh copper grid for 15 min. For

negative staining, 10 μL of 2% uranyl acetate was placed on the grid for 10 min, removed, and dried for 10 min at room temperature.

Western Blot Analysis

To evaluate EGFR expression levels in MDA-MB-231 and MDA-MB-453 cells, a Western blot analysis was performed. The cells were seeded in 6-well plates (2×10^5 cells per well) and lysed in a cell lysis buffer (RIPA buffer, Thermo Scientific, MA, USA) with a protease inhibitor (Thermo Scientific). For the analysis of CD47 expression in the transfected cells, cell lysates and CDNs were also lysed in the cell lysis buffer.

The lysates were separated by 10% SDS-PAGE and then transferred to nitrocellulose membranes. The membranes were blocked with skim milk in TBST and then incubated with a 1:1000 dilution of anti-EGFR rabbit antibodies (Cell Signaling Technology, Danvers, MA, USA) or anti-mouse CD47 antibodies (Invitrogen, Carlsbad, CA, USA). After washing, the membranes were treated with a 1:5000 dilution of horseradish peroxidase-conjugated goat anti-rabbit or goat anti-rat antibodies (Bethyl Laboratories, Montgomery, TX, USA). The membranes were washed and treated with SuperSignal® West Pico (Thermo Scientific). The immunoreactive bands were visualized using Fusion Solo Chemidoc (Vilber Lourmat, Deutschland, Germany).

In vitro Cytotoxicity Measurement

To evaluate the cytotoxicities of CDNs-DOX and iCDNs-DOX, MDA-MB-231 and MDA-MB-453 cells were seeded in 96-well plates (1×10^4 cells) and cultured for 48 h. The cancer cells were treated with various concentrations of CDNs-DOX and iCDNs-DOX (0, 0.001, 0.01, 0.1, 1, 10, and 100 μM DOX/mL) in 100 μL of serum-free media and incubated at 37°C for 48 h. Then, the cells were treated with 10 μL of Cell Counting Kit-8 (CCK8) solution (Dojindo Laboratories, Kumamoto, Japan) at 37°C for 2 h. The wells were characterized at 450 nm using an Infinite 200 Pro NanoQuant (TECAN). The IC_{50} (half-maximal inhibitory concentration) values were estimated using GraphPad Prism software (GraphPad Software, Inc., La Jolla, CA, USA).

In vitro Macrophage Uptake

The cellular uptake of CDNs and $CD47^+$-CDNs by RAW264.7 cells was evaluated using a FACSCalibur flow cytometer (BD Biosciences, San Jose, CA, USA) and a confocal laser scanning microscope (LSM 510; Zeiss, Heidenheim, Germany). RAW264.7 cells were seeded in 6-well plates (2×10^5 cells per well) and cultured for 12 h. CDNs and $CD47^+$-CDNs were fluorescently labeled with 3 μL of Vybrant ™ DiD Cell-Labeling Solution (Molecular Probes, Eugene, OR, USA) for 15 min at 37°C according to the manufacturer's protocol. The cells were treated with fluorescent CDNs or $CD47^+$-CDNs (1 μmole of phospholipids) and then analyzed at various time points using a FACSCalibur flow cytometer (Becton Dickinson, San Jose, CA, USA). At the same time points, the treated cells were viewed under a confocal microscope (LSM 510; Zeiss, Heidenheim, Germany).

In vitro EGFR-Dependent Cell Binding of iCDNs

MDA-MB-231 and MDA-MB-453 cells were seeded in 6-well plates and cultured for 48 h. After incubation, the cells were washed twice with L-15 (pH 7.4) and trypsinized with a trypsin-EDTA solution (pH 7.4). The cell pellet (1×10^5 cells) was suspended in L-15 in 5-mL polystyrene round-bottom tubes (Corning, New York, NY, USA). Alexa Fluor 488 (Invitrogen)-labeled anti-EGFR antibody-conjugated $CD47^+$-CDNs were added to the cells (50 μM phospholipids per tube) and incubated for 1 h at 4°C with continuous agitation. The binding of immuno-$CD47^+$-CDNs to the cells was analyzed using a FACSCalibur flow cytometer (Becton Dickinson).

To verify the cellular uptake of immuno-$CD47^+$-CDNs-DOX, the prepared immuno-$CD47^+$-CDNs containing DOX were added to the cells (50 μM phospholipids per tube) and then incubated for 0.5, 1, 4, or 24 h at 37°C in a serum-free medium. After incubation, the cells were washed twice with cold PBS (pH 7.4) and fixed with 2% paraformaldehyde. The cells were stained with 4.6-diamidino-2-phenylindole (DAPI) solution (Vector Lab, Burlingame, CA, USA) for 30 min in the dark and mounted on slides. The slides were observed using a confocal microscope.

In vivo Biodistribution of iCDNs

To examine the efficacy of iCDNs in drug delivery systems, we identified the in vivo biodistribution of the particles in mice. To prepare the tumor xenograft mouse model, six-week-old female BALB/c nude mice (Orient Bio, Seongnam, Korea) were subcutaneously injected with 200 μL of MDA-MB-231 cells (1×10^7) in a medium mixed with Matrigel (BD Biosciences) (1:1 volume ratio) at the mammary fat pad. The length and width of the tumors were measured with Vernier calipers, and tumor volumes were calculated as (length × width^2)/2.

When the tumor volumes reached approximately 200 mm^3, the rhodamine B-labeled CDNs, CD47$^+$-CDNs, or immuno-CD47$^+$-CDNs (10 mg lipid/kg) were injected into the mice via the tail vein (n=3). The mice were sacrificed 24 h later and major organs including tumors were immediately removed, followed by the measurement of their fluorescence intensity using a Maestro 2 in vivo imaging system (Caliper Life Sciences, Hopkinton, MA, USA).

In vivo Tumor Growth Inhibition by iCDNs-DOX

For the in vivo evaluation of the anticancer effect of iCDNs-DOX, mice were injected with MDA-MB-231 cells as described above and were treated with saline, free DOX, CD47$^-$ CDNs-DOX, CD47$^+$ CDNs-DOX, or iCDNs-DOX when the tumor volumes reached approximately 150 mm^3. The treatment was repeated three times at three-day intervals (3 mg DOX /kg, n=4). The tumor volume and bodyweight of the mice were measured at three-day intervals.

All mice were sacrificed on day 39 post-injection, and the liver, heart, kidneys, lungs, and tumors were collected, fixed with 10% formalin solution, embedded in paraffin, and sectioned for histological analysis. The sectioned tissues were stained with H&E and viewed under a microscope.

Acknowledgments

This research was supported by the National Research Foundation of Korea (NRF-2020R1F1A1069625; 2018R1C1B6007594), and the "Leaders in Industry-university Cooperation (LINC)" Project, supervised by the Ministry of Education (2020-51-0264).

Author Contributions

All authors made a significant contribution to the work reported, whether that is in the conception, study design, execution, acquisition of data, analysis and interpretation, or in all these areas; took part in drafting, revising or critically reviewing the article; gave final approval of the version to be published; have agreed on the journal to which the article has been submitted; and agree to be accountable for all aspects of the work.

Disclosure

The authors have declared conflicts of interest in relation to this work.

References

1. Krishnamurthy S, Vaiyapuri R, Zhang L, Chan JM. Lipid-coated polymeric nanoparticles for cancer drug delivery. *Biomater Sci*. 2015;3(7):923–936. doi:10.1039/C4BM00427B
2. Krishnamurthy S, Ke X, Yang YY. Delivery of therapeutics using nanocarriers for targeting cancer cells and cancer stem cells. *Nanomedicine*. 2015;10(1):143–160. doi:10.2217/nnm.14.154
3. Hanafy NAN, Quarta A, Ferraro MM, et al. Polymeric nano-micelles as novel cargo-carriers for LY2157299 liver cancer cells delivery. *Int J Mol Sci*. 2018;19(3):748. doi:10.3390/ijms19030748
4. Hanafy NAN, Quarta A, Di Corato R, et al. Hybrid polymeric-protein nano-carriers (HPPNC) for targeted delivery of TGFbeta inhibitors to hepatocellular carcinoma cells. *J Mater Sci Mater Med*. 2017;28(8):120. doi:10.1007/s10856-017-5930-7
5. Gagliardi M. Biomimetic and bioinspired nanoparticles for targeted drug delivery. *Ther Deliv*. 2017;8(5):289–299. doi:10.4155/tde-2017-0013
6. Zolnik BS, Gonzalez-Fernandez A, Sadrieh N, Dobrovolskaia MA. Nanoparticles and the immune system. *Endocrinology*. 2010;151(2):458–465. doi:10.1210/en.2009-1082
7. Krishnamurthy S, Gnanasammandhan MK, Xie C, Huang K, Cui MY, Chan JM. Monocyte cell membrane-derived nanoghosts for targeted cancer therapy. *Nanoscale*. 2016;8(13):6981–6985. doi:10.1039/C5NR07588B
8. Rao L, Bu LL, Xu JH, et al. Red blood cell membrane as a biomimetic nanocoating for prolonged circulation time and reduced accelerated blood clearance. *Small*. 2015;11(46):6225–6236. doi:10.1002/smll.201502388
9. Peng LH, Zhang YH, Han LJ, et al. Cell membrane capsules for encapsulation of chemotherapeutic and cancer cell targeting in vivo. *ACS Appl Mater Interfaces*. 2015;7(33):18628–18637. doi:10.1021/acsami.5b05065

10. Goh WJ, Lee CK, Zou S, Woon EC, Czarny B, Pastorin G. Doxorubicin-loaded cell-derived nanovesicles: an alternative targeted approach for anti-tumor therapy. *Int J Nanomedicine*. 2017;12:2759–2767. doi:10.2147/IJN.S131786
11. Roth JC, Curiel DT, Pereboeva L. Cell vehicle targeting strategies. *Gene Ther*. 2008;15(10):716–729. doi:10.1038/gt.2008.38
12. Ren H, Liu JQ, Li YQ, et al. Oxygen self-enriched nanoparticles functionalized with erythrocyte membranes for long circulation and enhanced phototherapy. *Acta Biomater*. 2017;59:269–282. doi:10.1016/j.actbio.2017.06.035
13. Oldenborg PA. CD47: a cell surface glycoprotein which regulates multiple functions of hematopoietic cells in health and disease. *ISRN Hematol*. 2013;2013:614619. doi:10.1155/2013/614619
14. Oldenborg PA, Zheleznyak A, Fang YF, Lagenaur CF, Gresham HD, Lindberg FP. Role of CD47 as a marker of self on red blood cells. *Science*. 2000;288(5473):2051–2054. doi:10.1126/science.288.5473.2051
15. Jaiswal S, Jamieson CH, Pang WW, et al. CD47 is upregulated on circulating hematopoietic stem cells and leukemia cells to avoid phagocytosis. *Cell*. 2009;138(2):271–285. doi:10.1016/j.cell.2009.05.046
16. Rivera A, Fu X, Tao L, Zhang X. Expression of mouse CD47 on human cancer cells profoundly increases tumor metastasis in murine models. *BMC Cancer*. 2015;15:964. doi:10.1186/s12885-015-1980-8
17. Gheibi Hayat SM, Bianconi V, Pirro M, Sahebkar A. Stealth functionalization of biomaterials and nanoparticles by CD47 mimicry. *Int J Pharm*. 2019;569:118628. doi:10.1016/j.ijpharm.2019.118628
18. Fang J, Nakamura H, Maeda H. The EPR effect: unique features of tumor blood vessels for drug delivery, factors involved, and limitations and augmentation of the effect. *Adv Drug Deliv Rev*. 2011;63(3):136–151. doi:10.1016/j.addr.2010.04.009
19. Li D, Chen X, Wang H, et al. Cetuximab-conjugated nanodiamonds drug delivery system for enhanced targeting therapy and 3D Raman imaging. *J Biophotonics*. 2017;10(12):1636–1646. doi:10.1002/jbio.201700011
20. Byrne JD, Betancourt T, Brannon-Peppas L. Active targeting schemes for nanoparticle systems in cancer therapeutics. *Adv Drug Deliv Rev*. 2008;60 (15):1615–1626. doi:10.1016/j.addr.2008.08.005
21. Messa C, Russo F, Caruso MG, Di Leo A. EGF, TGF-alpha, and EGF-R in human colorectal adenocarcinoma. *Acta Oncol*. 1998;37(3):285–289. doi:10.1080/028418698429595
22. Liao AH, Chou HY, Hsieh YL, Hsu SC, Wei KC, Liu HL. Enhanced Therapeutic Epidermal Growth Factor Receptor (EGFR) antibody delivery via pulsed ultrasound with targeting microbubbles for glioma treatment. *J Med Biol Eng*. 2015;35(2):156–164. doi:10.1007/s40846-015-0032-9
23. Wicki A, Ritschard R, Loesch U, Deuster S, Rochlitz C, Mamot C. Large-scale manufacturing of GMP-compliant anti-EGFR targeted nanocarriers: production of doxorubicin-loaded anti-EGFR-immunoliposomes for a first-in-man clinical trial. *Int J Pharm*. 2015;484(1–2):8–15. doi:10.1016/j.ijpharm.2015.02.034
24. Cho YS, Yoon TJ, Jang ES, et al. Cetuximab-conjugated magneto-fluorescent silica nanoparticles for in vivo colon cancer targeting and imaging. *Cancer Lett*. 2010;299(1):63–71. doi:10.1016/j.canlet.2010.08.004
25. Liao C, Sun Q, Liang B, Shen J, Shuai X. Targeting EGFR-overexpressing tumor cells using Cetuximab-immunomicelles loaded with doxorubicin and superparamagnetic iron oxide. *Eur J Radiol*. 2011;80(3):699–705. doi:10.1016/j.ejrad.2010.08.005
26. Vanneman M, Dranoff G. Combining immunotherapy and targeted therapies in cancer treatment. *Nat Rev Cancer*. 2012;12(4):237–251. doi:10.1038/nrc3237
27. Gao C, Lin Z, Jurado-Sanchez B, Lin X, Wu Z, He Q. Stem cell membrane-coated nanogels for highly efficient in vivo tumor targeted drug delivery. *Small*. 2016;12(30):4056–4062. doi:10.1002/smll.201600624
28. Xuan M, Shao J, Dai L, He Q, Li J. Macrophage cell membrane camouflaged mesoporous silica nanocapsules for in vivo cancer therapy. *Adv Healthc Mater*. 2015;4(11):1645–1652. doi:10.1002/adhm.201500129
29. Fang RH, Hu CM, Luk BT, et al. Cancer cell membrane-coated nanoparticles for anticancer vaccination and drug delivery. *Nano Lett*. 2014;14 (4):2181–2188. doi:10.1021/nl500618u
30. Liu XS, Jiang JH, Meng H. Transcytosis - An effective targeting strategy that is complementary to "EPR effect" for pancreatic cancer nano drug delivery. *Theranostics*. 2019;9(26):8018–8025. doi:10.7150/thno.38587
31. Bertrand N, Wu J, Xu X, Kamaly N, Farokhzad OC. Cancer nanotechnology: the impact of passive and active targeting in the era of modern cancer biology. *Adv Drug Deliv Rev*. 2014;66:2–25. doi:10.1016/j.addr.2013.11.009
32. Kim MW, Jeong HY, Kang SJ, et al. Anti-EGF receptor aptamer-guided co-delivery of anti-cancer siRNAs and quantum dots for theranostics of triple-negative breast cancer. *Theranostics*. 2019;9(3):837–852. doi:10.7150/thno.30228
33. Puri C, Tosoni D, Comai R, et al. Relationships between EGFR signaling-competent and endocytosis-competent membrane microdomains. *Mol Biol Cell*. 2005;16(6):2704–2718. doi:10.1091/mbc.e04-07-0596
34. Wang YY, Wang YD, Chen GJ, Li YT, Xu W, Gong SQ. Quantum-dot-based theranostic micelles conjugated with an anti-EGFR nanobody for triple-negative breast cancer therapy. *ACS Appl Mater Interfaces*. 2017;9(36):30297–30305. doi:10.1021/acsami.7b05654
35. Yang B, Zhang S, Fang X, Kong JL. Double signal amplification strategy for ultrasensitive electrochemical biosensor based on nuclease and quantum dot-DNA nanocomposites in the detection of breast cancer 1 gene mutation. *Biosens Bioelectron*. 2019;142:111544. doi:10.1016/j.bios.2019.111544
36. Kang SJ, Jeong HY, Kim MW, et al. Anti-EGFR lipid micellar nanoparticles co-encapsulating quantum dots and paclitaxel for tumor-targeted theranosis. *Nanoscale*. 2018;10(41):19338–19350. doi:10.1039/C8NR05099F
37. Wiles ME, Bell C, Landfair D, Lynam E, Bendele RA. Anthracycline efficacy in vitro: cytotoxicity of liposomal/nonliposomal daunorubicin and doxorubicin for multiple tumor cell types. *Drug Deliv*. 1997;4(4):255–262. doi:10.3109/10717549709052011
38. Tomas A, Futter CE, Eden ER. EGF receptor trafficking: consequences for signaling and cancer. *Trends Cell Biol*. 2014;24(1):26–34. doi:10.1016/j.tcb.2013.11.002
39. Stewart JC. Colorimetric determination of phospholipids with ammonium ferrothiocyanate. *Anal Biochem*. 1980;104(1):10–14. doi:10.1016/0003-2697(80)90269-9
40. Fritze A, Hens F, Kimpfler A, Schubert R, Peschka-Suss R. Remote loading of doxorubicin into liposomes driven by a transmembrane phosphate gradient. *Biochim Biophys Acta Biomembranes*. 2006;1758(10):1633–1640. doi:10.1016/j.bbamem.2006.05.028